Observation of Anomalous Diffusion and Lévy Flights in a Two-Dimensional Rotating Flow

T. H. Solomon,* Eric R. Weeks, and Harry L. Swinney†
Center for Nonlinear Dynamics and Department of Physics, University of Texas at Austin, Austin, Texas 78712
(Received 17 September 1993)

Chaotic transport in a laminar fluid flow in a rotating annulus is studied experimentally by tracking large numbers of tracer particles for long times. Sticking and unsticking of particles to remnants of invariant surfaces (Cantori) around vortices results in superdiffusion: The variance of the displacement grows with time as t^γ with $\gamma = 1.65 \pm 0.15$. Sticking and flight time probability distribution functions exhibit power-law decays with exponents 1.6 ± 0.3 and 2.3 ± 0.2, respectively. The exponents are consistent with theoretical predictions relating Lévy flights and anomalous diffusion.

PACS numbers: 47.52.+j, 47.32.–y, 51.20.+d, 92.10.Lq

Transport in a fluid flow can be characterized by the variance of the displacement of a distribution of tracer particles, $\sigma^2 \sim \langle (\Delta r)^2 \rangle$, which for normal diffusive processes grows linearly with time: $\sigma^2 \sim t^\gamma$ with $\gamma = 1$. Processes with $\gamma \neq 1$ are termed anomalous diffusion [1,2]. Subdiffusion ($0 < \gamma < 1$) occurs in flows with well-defined "sticking" regions that retard the motion of fluid elements or tracer particles. Sticking can occur in two-dimensional cellular flows if molecular diffusion is large enough [3] or if the flow is time dependent [4,5]. In the latter case, trajectories of passive tracer particles are typically chaotic (exponential separation of nearby particles) [6], and remnants of invariant surfaces (Cantori) cause long sticking times with a power-law rather than exponential distribution [4,5].

Superdiffusion ($1 < \gamma < 2$) can occur if tracer trajectories in the flow have long excursions ("Lévy flights") [1,2,7,8]. Lévy flights, defined by flight length probability distributions with divergent second moments (e.g., power-law distribution functions), are well known mathematically [1]. One signature of superdiffusion, fractal scaling of trajectories, has been found in analyses of floating tracers in ocean [9] and surface wave [10] flows, but these flows were turbulent and difficult to characterize, so the mechanisms responsible for the anomalous behavior were unclear. Moreover, those experiments did not follow enough particle trajectories to determine the sticking or flight time statistics. Superdiffusive behavior was also found in a recent experiment on micelles, and that behavior was modeled as a Lévy process [11].

We have made direct measurements of Lévy flights and superdiffusion. The experiments study transport in a time-periodic flow composed of a circular chain of vortices in a rapidly rotating annulus; see Fig. 1(a). The flow is almost perfectly two dimensional; hence the stream function for the velocity field is a Hamiltonian and the equations of motion for a tracer particle in the flow are Hamilton's equations [12]. Even though the velocity field is laminar, passive tracers in the flow can have chaotic trajectories ("chaotic advection" [6]), intermittently sticking near the vortices and then moving large distances in the jet regions that sandwich the vortex chain. We have used digital image processing techniques [13] to track simultaneously up to 100 neutrally buoyant particles in the flow for times much longer than typical time scales of the velocity field. Digitized trajectories are used to calculate the variance of the displacement of tracer particles and the sticking and flight time probability distributions.

The apparatus is an annular tank rotating at a frequency of 1.5 Hz. The inner and outer radii are 10.8 and 43.2 cm, respectively, and the depths at these radii are 17.1 and 20.3 cm [12,14]. The annulus is filled completely with a 38% glycerol solution (by weight) in water with kinematic viscosity 0.030 cm^2/s. Fluid is pumped at 45 cm^2/s into the tank through a ring of radius 18.9 cm and from the tank through a ring of radius 35.1 cm; the source and sink rings each consist of 120 holes (0.26 cm diameter) in the bottom of the tank. The action of the Coriolis force on the pumped fluid results in a counterrotating azimuthal jet with shear layers above each ring. Instability of the inner shear layer is inhibited by inserting into the tank a 6 cm tall annular Plexiglas barrier with inner and outer radii of 10.8 and 19.4 cm, respectively. The axisymmetric inner shear layer is then embedded in the Stewartson layer at the edge of the barrier.

The outer shear layer is unstable, leading to the formation of a circular chain of vortices that slowly rotates with respect to the annulus. The resultant flow has a periodic time dependence as measured by hot film probes mounted in the lid of the tank. In a reference frame corotating with the vortex chain, this flow would be time independent with all particle trajectories following closed stream lines—there would be no chaotic trajectories. This basic flow is perturbed to obtain the flow that we have studied, one with chaotic particle trajectories: nonaxisymmetric forcing is produced by pumping through one 60° arc of holes (both outer and inner rings) at a rate less than 50% of that for the remainder of the holes. Thus as each vortex moves around the annulus, it undergoes an amplitude oscillation with a period equal to its propagation time around the annulus (70.0 s); this oscillation period is comparable to a typical vortex turnover time (25 s). The resultant flow is simply periodic in the

0031-9007/93/71(24)/3975(4)$06.00

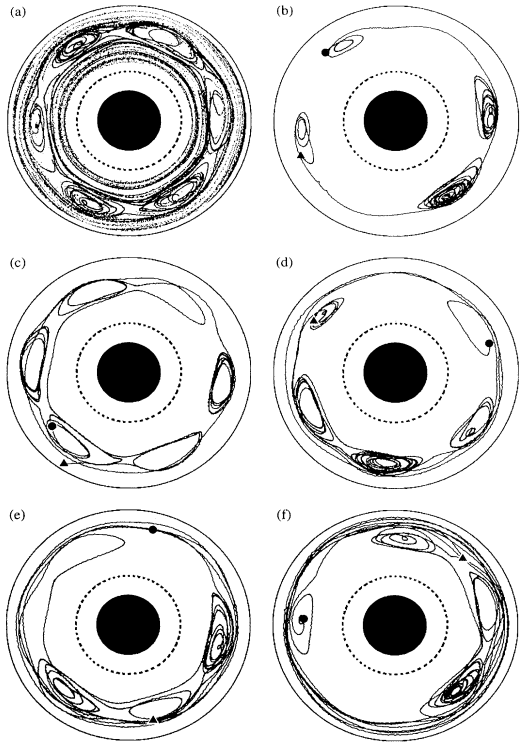

FIG. 1. (a) Streaks formed by 90 s long trajectories of 40 particles reveal the presence of six vortices. (b)–(f) Individual particle trajectories of duration 800–1500 s. The beginning of each trajectory is marked by a circle, the end by a triangle. Long sticking events can be seen in each case, and flights of length at least equal to one rotation around the annulus can be seen in each case except (b). Hyperbolic fixed points, near which the particle motion is particularly sensitive to transitions between flights and sticking events, are evident in (c) and (e). In each of these figures, the tracer motion is viewed from a reference frame that is corotating with the vortex chain, which rotates with a frequency 0.01429 Hz slower than the 1.5 Hz rotation frequency of the annulus. The inner and outer circles represent the annulus boundaries, and the dashed circle denotes the outer edge of the Plexiglas barrier.

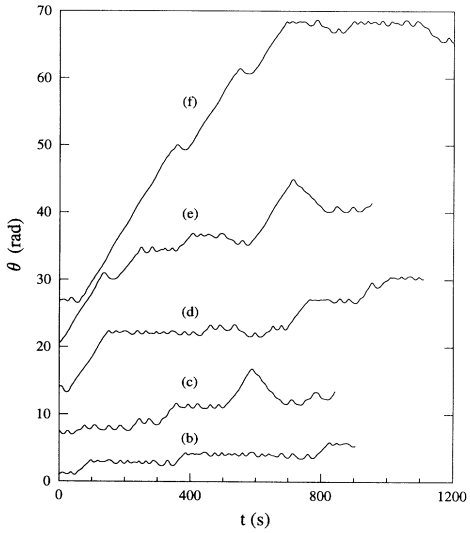

FIG. 2. The azimuthal displacement as a function of time for the particle trajectories in Figs. 1(b)–1(f). Oscillations about horizontal lines are sticking events; e.g., in the first long sticking event for trajectory (d), the particle makes 10.5 rotations about a vortex before escaping. Diagonal lines are flights between the sticking events. The starting angle $\theta(t = 0)$ is arbitrary in this plot.

corotating reference frame of the vortex chain, but particles advected by this flow can have chaotic trajectories.

Neutrally buoyant tracer particles are suspended in the flow and are tracked for up to 30 min. The particles are made from mixtures of fluorescent crayons and concrete powder, ground and sieved to a size of approximately 1 mm. The Stokes number [15] for the particles is approximately 0.002 for vortex length scales, insuring that they follow the flow faithfully on these length scales. The visibility time is limited by a very slow vertical drift of the particles through the illuminated section, due mainly to Ekman pumping in the vortices [14].

A chain of six vortices is clearly visible in Fig. 1(a). Figures 1(b)–1(f) show individual particle trajectories of duration 800–1500 s. In a plot of the corresponding azimuthal displacements (Fig. 2), flights appear as steep diagonal lines and sticking events are oscillations about horizontal lines. Note the long flights, particularly in (f), and the long sticking times, particularly in (b) and (d). The velocity of a particle is approximately constant, except when it slows down as it passes near hyperbolic points. The approximate constancy of the azimuthal component of velocity can be seen in the slopes of the plots in Fig. 2. There are many more flights in the corotating direction (corresponding to motion outside the vortex chain) than in the counterrotating direction; this asymmetry is probably due to the curvature of the system, which causes the separatrices outside the vortex chain to be longer and more curved than those inside the chain [16].

Transport in this system is analyzed in the azimuthal direction, with the variance given by $\sigma^2(t) = \langle(\theta - \langle\theta\rangle)^2\rangle$; see Fig. 3. In the calculations, the initial angle $\theta(t = 0)$ is defined to be zero for each trajectory. Only those trajectories that display both sticking events and flights are used in the calculations of σ^2. The data are less accurate at large t since there are more short flights than long flights. The slope γ of a log-log plot of $\sigma^2(t)$ has a plateau at $\gamma = 1.65 \pm 0.15$ for long times (> 20 s), indicating superdiffusion.

Sticking and flight time probability distribution functions (PDFs) of tracers are determined from analyses of data for $\theta(t)$. A flight is identified by $\Delta\theta > \pi/3$ (angular width of one vortex) between successive extrema. The sticking events are then simply the intervals between

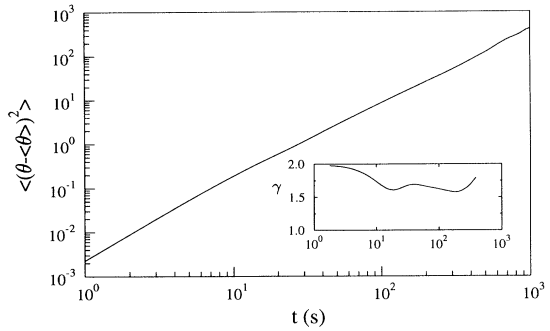

FIG. 3. Variance of the azimuthal displacement of a distribution of tracer particles for a time-periodic laminar flow. The slope, shown in the inset, has a plateau that yields the exponent for the power-law growth, $\gamma = 1.65 \pm 0.15$ (superdiffusion).

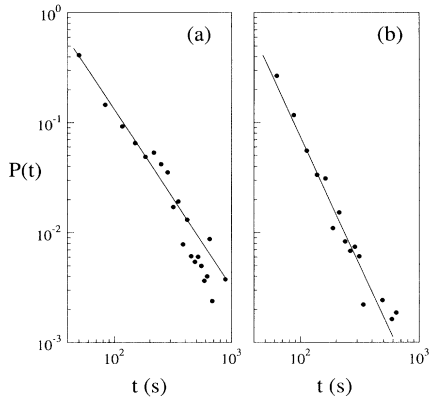

FIG. 4. (a) Sticking time probability distribution, which exhibits power-law decay for $t < 300$ s with exponent (slope) $\nu = 1.6 \pm 0.3$. (b) Flight time probability distribution function, which is a power law with exponent $\mu = 2.3 \pm 0.2$.

flights. The PDFs are determined from normalized histograms of the duration of these events. A small correction is required to compensate for the finite duration of the measured trajectories, which biases the data in favor of shorter sticking/flight events. This correction is determined by creating artificial (numerical) trajectories with algebraic flight and sticking PDFs, chopping them (randomly) into finite trajectories with durations comparable to those observed in the experiment, and comparing the PDFs obtained from these finite trajectories to the expected PDFs (for infinite duration trajectories).

A histogram of sticking times [Fig. 4(a)] indicates a power-law relation, $P_s(t) \sim t^{-\nu}$, with $\nu = 1.6 \pm 0.3$ [17]. There is a slight dropoff in the PDF for $t > 300$ s, possibly indicative of a transition to exponential decay at large times. Theoretical studies [5,18] predict that long-term sticking (power law PDFs) in Hamiltonian systems is a consequence of a characteristic hierarchical island structure. The dropoff in our PDF for large t probably arises because noise and the finite tracer particle size [15] mask the island structure beyond the second or third generation of islands. Numerical studies of sticking in a variety of systems have yielded a wide range of values (0.7–3.8) for the sticking exponent [4,5,19].

The flight times also have power-law distributions [Fig. 4(b)], $P_f(t) \sim t^{-\mu}$ with $\mu = 2.3 \pm 0.2$ [17], which indicates that the trajectories can be described quantitatively as Lévy flights. The PDF in Fig. 4(b) includes data from both corotating and counterrotating flights; the corotating and counterrotating flights both have power-law PDFs with the same decay exponent. Flight *length* distributions are also algebraic with the same exponent, further indicating that the flight lengths and durations are linearly related.

The connection between Lévy motion and anomalous diffusion has been analyzed theoretically for model systems [7,20] and these analyses yield an exponent $\gamma = 4 - \mu$, assuming constant flight velocity. Our measured values of μ (2.3) and γ (1.65) are in good accord with this relation, which assumes that γ is dominated by the flight statistics. A recent analysis of a Hamiltonian model [21] yields a dependence of the growth of the variance on both flight and sticking statistics: $\gamma = 2\nu/(\mu - 1)$. This result is also consistent with the experimental data, given the uncertainty in our exponent values.

For contrast we have also examined transport in a weakly turbulent velocity field that contains no persistent vortices and no jets encircling the annulus. The turbulent flow was produced by pumping through only the outer circle of holes with the direction of pumping alternating for successive sectors of 60° width; the total pumping rate was fixed at 45 cm^3/s, as before, but the water-glycerol mixture was replaced with water (kinematic viscosity 0.009 cm^2/s) to achieve a larger Reynolds number.

The absence of well-defined flights and sticking events in the turbulent flow is evident in Figs. 5(a) and 5(b), which contrast with Figs. 1 and 2 for the laminar flow. In the turbulent flow the slope of the variance of the azimuthal displacement, shown in Fig. 5(c), decreases monotonically with time and appears to approach the value expected for normal diffusion, $\gamma = 1$, but we cannot track particles long enough to determine the asymptotic behavior.

In conclusion, by following the trajectories of large numbers of particles for long times we have been able to obtain direct evidence for Lévy flights and anomalous diffusion. Chaotic advection of passive tracer particles in our laminar flow results in alternating sticking events and long-range flights, each with power-law probability distributions. For the particular case we have considered in detail, the transport of an ensemble of tracers is superdiffusive with a variance that grows with time with exponent $\gamma = 1.65$. Future experiments will examine the dependence of the power-law exponents γ, μ, and ν on parameters for flows ranging from periodic to fully tur-

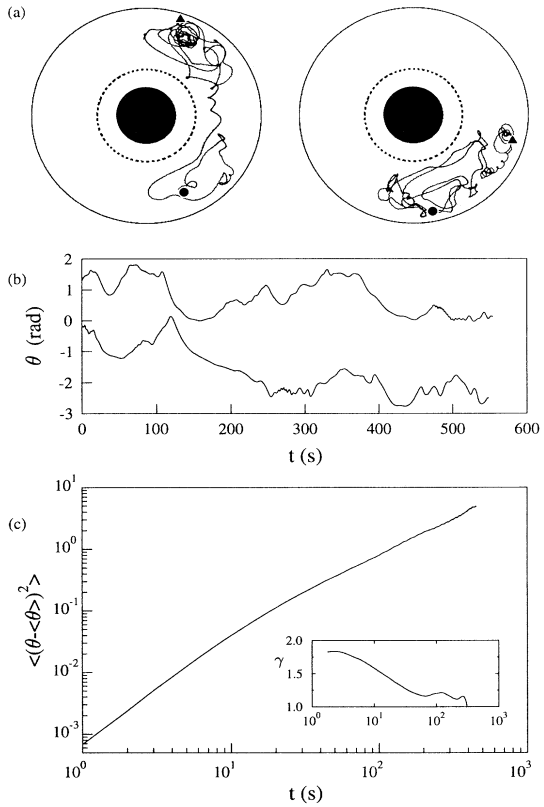

FIG. 5. Transport in a weakly turbulent flow with no jet region. (a) Two particle trajectories of about 500 s duration. (b) The azimuthal displacement as a function of time for the particle trajectories in (a). Since there are no long-range flights, the total displacement in 500 s is typically an order of magnitude smaller here than for the laminar flow; compare Fig. 2. The starting angle $\theta(t = 0)$ is arbitrary in this plot. (c) Variance of the azimuthal displacement of an ensemble of tracer particles. The slope, shown in the inset, decreases monotonically toward unity and has no plateau, in contrast to the case for superdiffusion; compare Fig. 3.

bulent. We hope that this work will stimulate theoretical studies of anomalous diffusion in both Hamiltonian and dissipative systems.

We are pleased to acknowledge the assistance of M. S. Pervez and helpful discussions with D. del-Castillo-Negrete, P. J. Morrison, E. Ott, M. F. Shlesinger, W. R. Young, and G. M. Zaslavsky. This work was supported by the Office of Naval Research Grant No. N00014-89-J-1495.

* Current address: Department of Physics, Bucknell University, Lewisburg, PA 17837. Electronic address: tsolomon@bucknell.edu

† Electronic address: swinney@chaos.utexas.edu

[1] B. D. Hughes, M. F. Shlesinger, and E. W. Montroll, Proc. Natl. Acad. Sci. U.S.A. **78**, 3287 (1981); E. W. Montroll and M. F. Schlesinger, in *Nonequilibrium Phenomena II: From Stochastics to Hydrodynamics*, Studies in Statistical Mechanics Vol. II, edited by J. L. Lebowitz and E. W. Montroll (North-Holland, Amsterdam, 1984), p. 1.

[2] M. F. Shlesinger, G. M. Zaslavsky, and J. Klafter, Nature (London) **363**, 31 (1993).

[3] W. Young, A. Pumir, and Y. Pomeau, Phys. Fluids A **1**, 462 (1989); O. Cardoso and P. Tabeling, Eur. J. Mech. B/Fluids **8**, 459 (1989).

[4] C. F. F. Karney, Physica (Amsterdam) **8D**, 360 (1983); B. V. Chirikov and D. L. Shepelyansky, Physica (Amsterdam) **13D**, 395 (1984).

[5] J. D. Meiss and E. Ott, Phys. Rev. Lett. **55**, 2741 (1985); Physica (Amsterdam) **20D**, 387 (1986).

[6] H. Aref, J. Fluid Mech. **143**, 1 (1984).

[7] J. Klafter, A. Blumen, and M. F. Shlesinger, Phys. Rev. A **35**, 3081 (1987); X.-J. Wang, Phys. Rev. A **45**, 8407 (1992).

[8] G. M. Zaslavsky and M. K. Tippett, Phys. Rev. Lett. **67**, 3251 (1991); V. V. Afanasiev, R. Z. Sagdeev, and G. M. Zaslavsky, Chaos **1**, 143 (1991).

[9] M. G. Brown and K. B. Smith, Phys. Fluids A **3**, 1186 (1991); A. R. Osborne, A. D. Kirwan, A. Provenzale, and L. Bergamasco, Tellus **41A**, 416 (1989).

[10] R. Ramshankar and J. P. Gollub, Phys. Fluids A **3**, 1344 (1991).

[11] A. Ott, J. P. Bouchaud, D. Langevin, and W. Urbach, Phys. Rev. Lett. **65**, 2201 (1990).

[12] T. H. Solomon, W. J. Holloway, and H. L. Swinney, Phys. Fluids A **5**, 1971 (1993); R. P. Behringer, S. D. Meyers, and H. L. Swinney, Phys. Fluids A **3**, 1243 (1991).

[13] M. S. Pervez and T. H. Solomon (to be published).

[14] The geometry with a flat lid and sloping bottom are described more fully in J. Sommeria, S. D. Meyers, and H. L. Swinney, in *Nonlinear Topics in Ocean Physics*, edited by A. Osborne (North-Holland, Amsterdam, 1991), p. 227.

[15] S. Elghobashi and G.C. Truesdell, J. Fluid Mech. **242**, 655 (1992).

[16] D. del-Castillo-Negrete and P.J. Morrison, Phys. Fluids A **5**, 948 (1993).

[17] The uncorrected PDFs are described by power laws with $\nu = 1.9$ and $\mu = 2.8$.

[18] G. M. Zaslavsky, D. Stevens, and H. Weitzner, Phys. Rev. E **48**, 1683 (1993).

[19] Y.-C. Lai, R. Blümel, E. Ott, and C. Grebogi, Phys. Rev. Lett. **68**, 3491 (1992); C. F. Hillermeier, R. Blümel, and U. Smilansky, Phys. Rev. A **45**, 3486 (1992); J. B. Weiss and E. Knobloch, Phys. Rev. A **40**, 2579 (1989); C. Jung, T. Tel, and E. Ziemniak, Chaos (to be published); Y.-C. Lai, M. Ding, C. Grebogi, and R. Blümel, Phys. Rev. A **46**, 4661 (1992).

[20] T. Geisel, J. Nierwetberg, and A. Zacherl, Phys. Rev. Lett. **54**, 616 (1985).

[21] G. Zaslavsky (to be published).